Supporting Information

Tough Biomimetic Films for Harnessing Natural Evaporation for Various Self-powered Devices

Tian Yang, Honglin Yuan, Sitong Wang, Xuhan Gao, Huhu Zhao, Pengying Niu, Beibei Liu, Bo Li, Huanjun Li*

School of Chemistry and Chemical Engineering
Beijing Institute of Technology
100081, P. R. China
E-mail: lihj@bit.edu.cn

Table of Contents

1. Supplementary Figures, Table and Discussion..S3
2. Supporting Video Captions...S15
3. References S16

1. Supplementary Figures, Table and Discussion

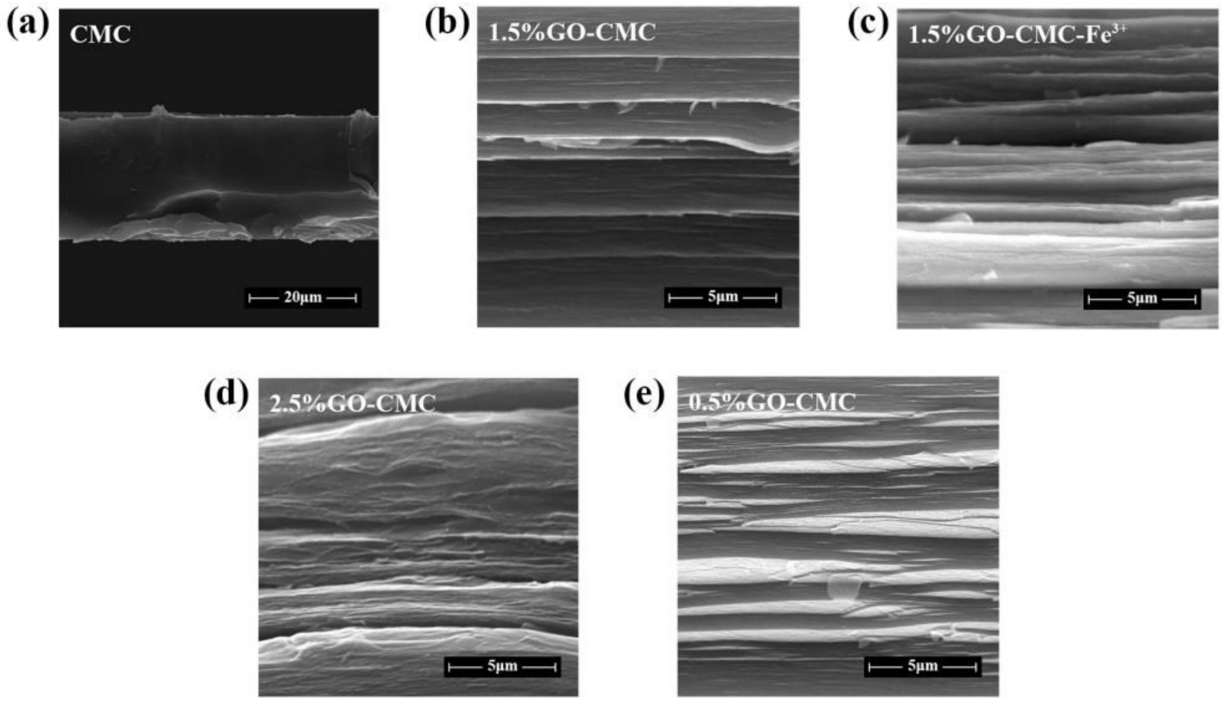

Figure S1. Cross-sectional SEM images of (a) CMC film, (b) 1.5% GO/CMC film, (c) 1.5% GO/CMC/Fe^{3+} film, (d) 2.5% GO/CMC film, (e) 0.5% GO/CMC film.

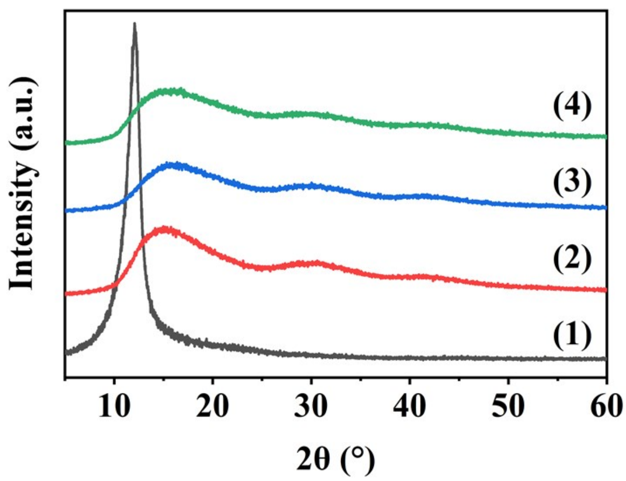

Figure S2. XRD patterns for (1) GO, (2) CMC, (3)1.5% GO/CMC, (4) 1.5% GO/CMC/Fe^{3+}.

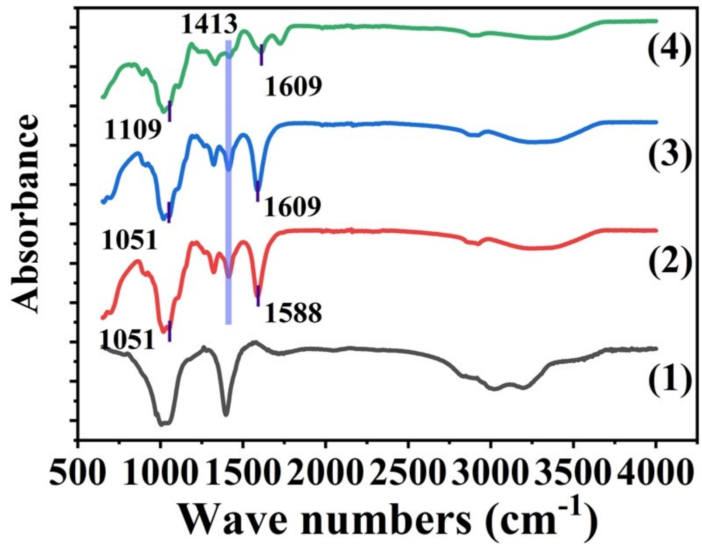

Figure S3. FTIR spectra of various films for (1) GO, (2) CMC, (3) 1.5% GO/CMC, (4) 1.5% GO/CMC/Fe^{3+}.

Fourier transform infrared (FTIR) spectra of GO, CMC, GO/CMC, and GO/CMC/Fe^{3+} films were shown in **Figure S3**. It is observed that the peak at 1588 cm^{-1} for C-O symmetrical mode of COO^{-1} of pure CMC shifts to 1609 cm^{-1} for the GO/CMC film, confirming the intermolecular hydrogen bonds between CMC and GO, which is in agreement with the previous report.[1] On the other hand, the decreased peak intensity of C-O asymmetrical mode at 1413 cm^{-1} and the peak shift from 1051 to 1109 cm^{-1} ascribed to C-O stretching mode of COO^{-1} are the direct evidence of ion-crosslinking between CMC and Fe^{3+}.

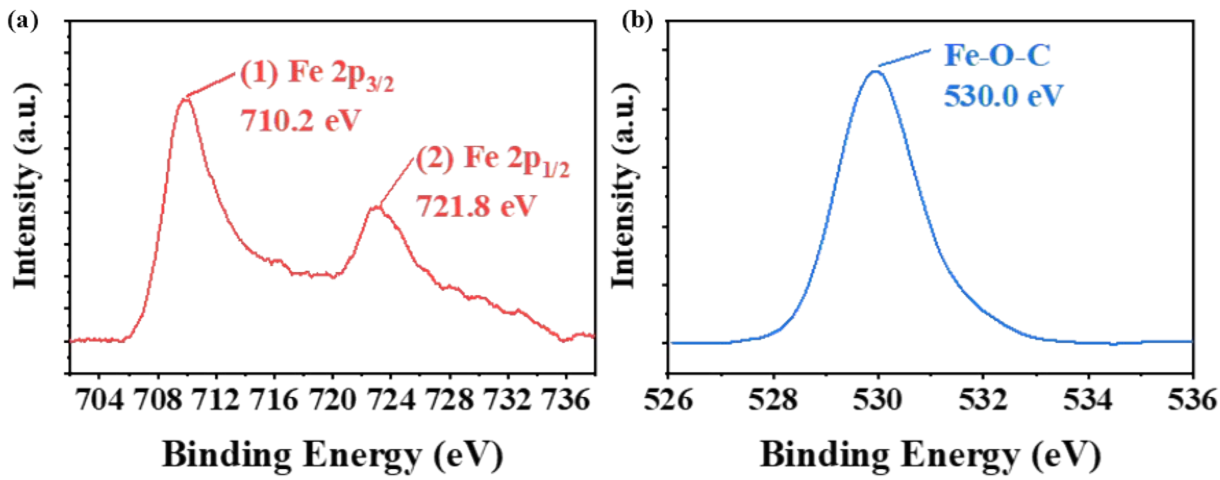

Figure S4. (a) Fe 2p XPS spectrum and (b) O 1s XPS spectrum for 1.5% GO/CMC/Fe^{3+} film.

The XPS analysis of the GO/CMC/Fe^{3+} film were further conducted to explore the interaction of CMC and Fe(III). It was found that there are two peaks at 710.2 eV and 721.8 eV, corresponding to the binding energies of Fe $2p_{1/2}$ and Fe $2p_{3/2}$ (**Figure S4a**). In addition, the strong peak at 530.0 eV of O 1s from Fe-O-C binding was observed (**Figure S4b**), demonstrating the ionic coordination interaction between CMC and Fe(III).

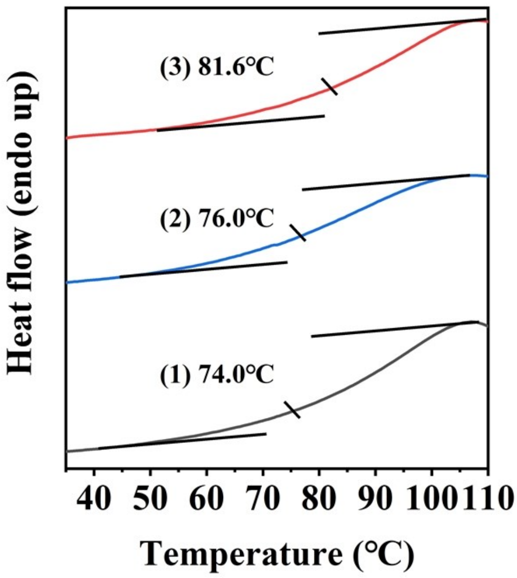

Figure S5. DSC curves for (1) CMC, (2)1.5%GO/CMC, (3) 1.5GO/CMC/Fe^{3+}

The influences of GO and Fe(III) cross-linking on the segmental motion of CMC chain in the film are analyzed from the DSC curves **(Figure S5)**. GO/CMC/Fe^{3+} film has a glass transition temperatures (T_g) of 81.6℃, which is higher than that of GO/CMC (76.0℃) and pure CMC film (74.0℃). The increase of T_g confirms the H-bonding interaction between GO and CMC[2–5] and the ionic crosslinking between CMC and Fe(III).

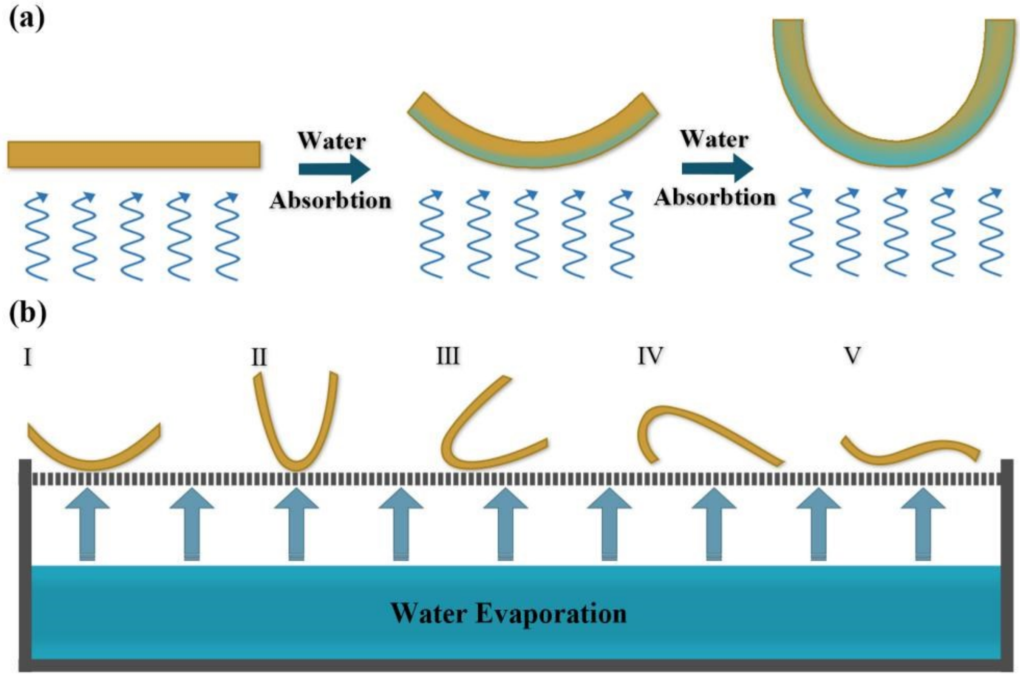

Figure S6. (a) Schematic illustration of the mechanical motion mechanism of the composite film driven by water gradient. (b) Sketches of multistage motion of the film on a porous substrate suspended above water surface.

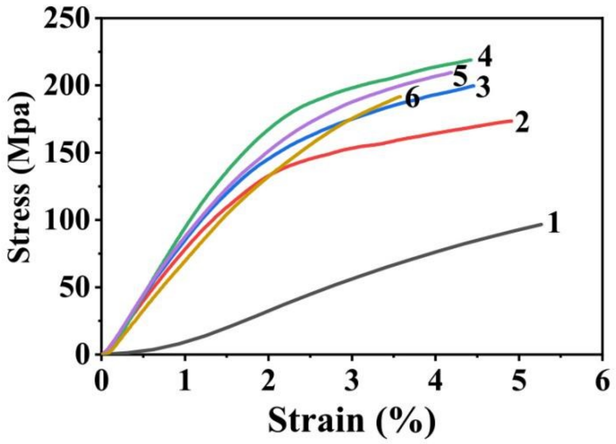

Figure S7. Typical stress-strain curves of CMC, 0.5% GO/CMC, 1.0% GO/CMC, 1.5% GO-CMC, 2.0% GO-CMC, 2.5% GO-CMC films corresponding to 1 to 6.

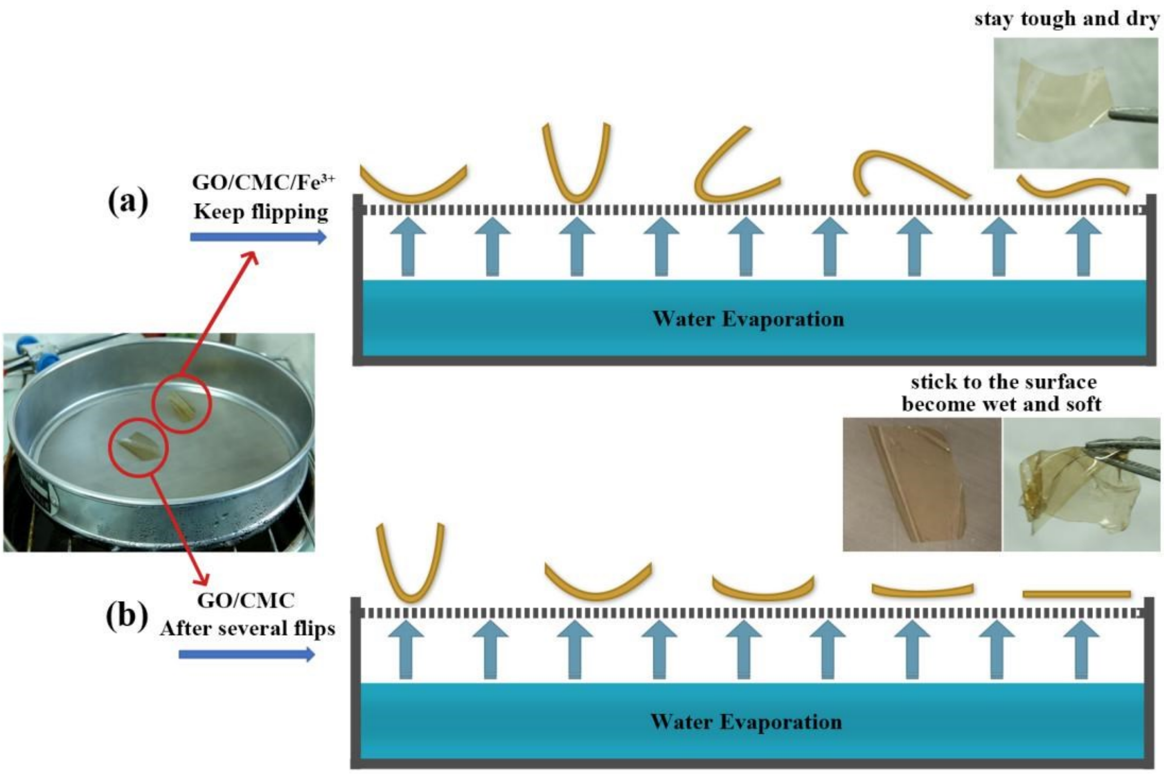

Figure S8. Comparison of the film actuator before and after ferric crosslinking: (a) The 1.5% GO/CMC/Fe^{3+} film keeps stable and continuous flipping motion; (b) GO/CMC film adhered to the porous substrate after several turnover.

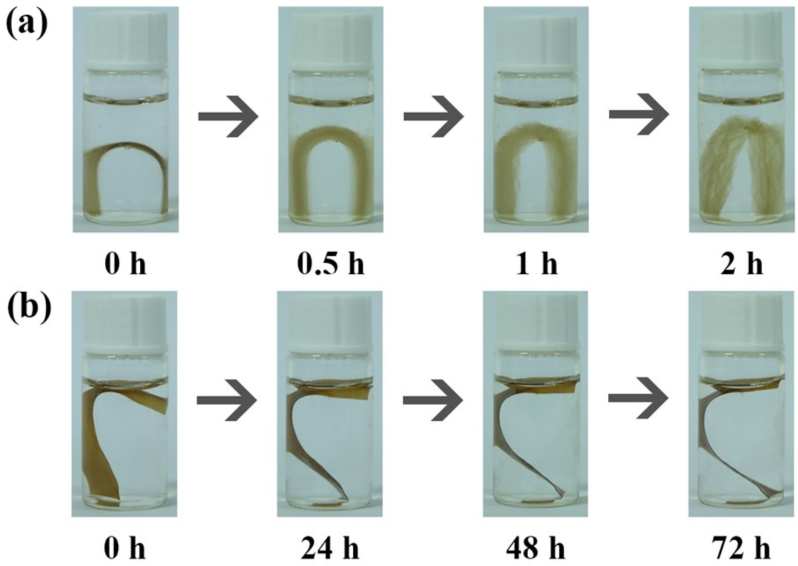

Figure S9. Comparison of water stability. (a) 1.5% GO/CMC film (b) 1.5% GO/CMC/Fe^{3+} film.

To further verify the effect of ionic crosslinking on water stability of 1.5% GO/CMC/Fe^{3+} film, which was immersed in water with the control sample (1.5% GO/CMC film). It was noted that the control sample dissolved after 2 h, while the 1.5% GO/CMC/Fe^{3+} film did not dissolve even after 72 h.

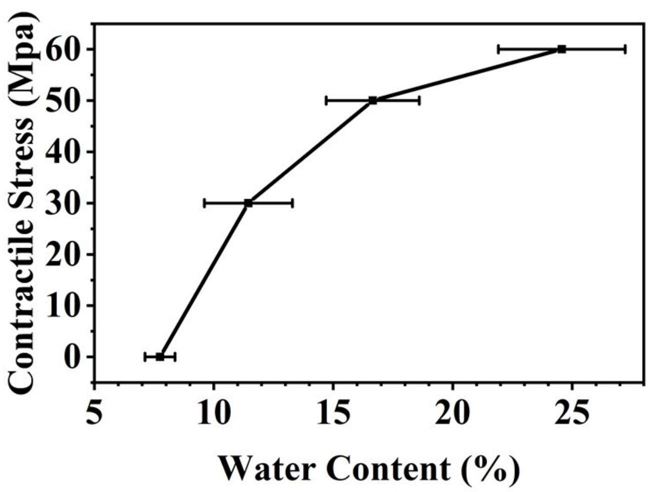

Figure S10. The relationship between the contractile stress and water content of a 20-μm 1.5% GO/CMC/Fe^{3+} film.

Contractile stress is generated by water absorption and dehydration. So contractile stress of the film is determined by the water content of both dry state (before absorption) and wet state (after absorption) of the actuator. Therefore we set the dry state of the actuator (before absorption) to its equilibrium state with the ambient humidity (~7.8% water content under 25°C, 20%RH). In such condition, contractile stress is only determined by the water content of the wet state of the actuator (after absorption). Then a plot showing the relationship between contractile stress and water content of the wet state of the actuator is conducted. **Figure S10** shows that when the water content of the film decreases from ~11.4%, ~16.7% and ~24.6% to ~7.8%, the contractile stress of about 30, 50 and 60Mpa will be generated respectively.

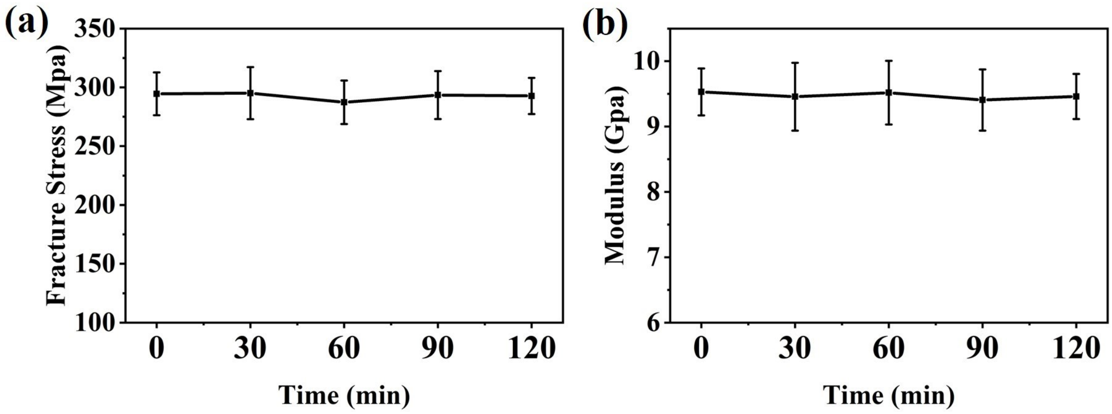

Figure S11. Effect of flipping time on fracture stress (a) and modulus (b) of the 20-µm 1.5% GO/CMC/Fe^{3+} film.

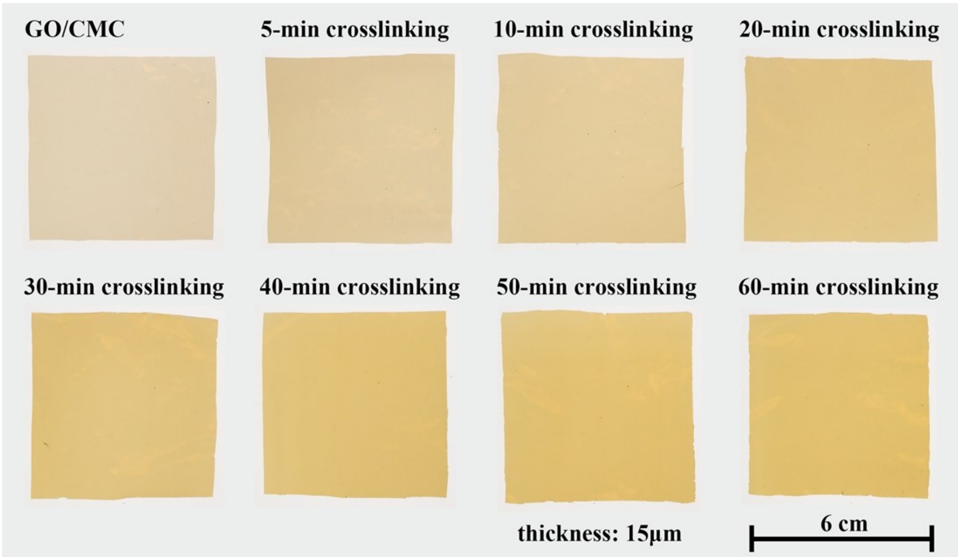

Figure S12. Effect of crosslinking time on 15-µm 1.5% GO/CMC/Fe^{3+} film.

With the increase of crosslinking time, the color of the film deepens and the crosslinking density increases. The film is placed on a backlight plate with the same brightness. The camera is set to a fixed setting to ensure comparability of the results.

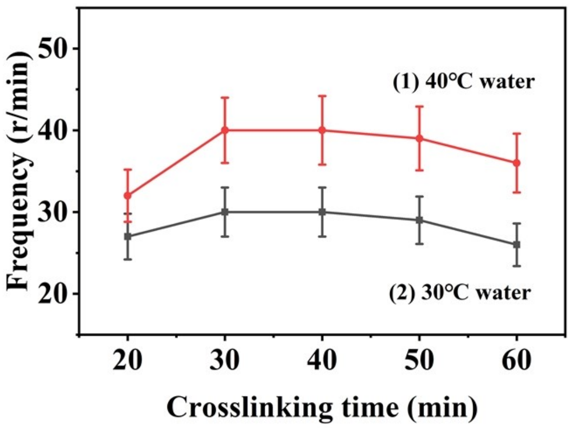

Figure S13. Effect of crosslinking time on the flipping frequency of 15-µm 1.5% GO/CMC/Fe^{3+} film over 40℃ water (1) and 30℃ water (2).

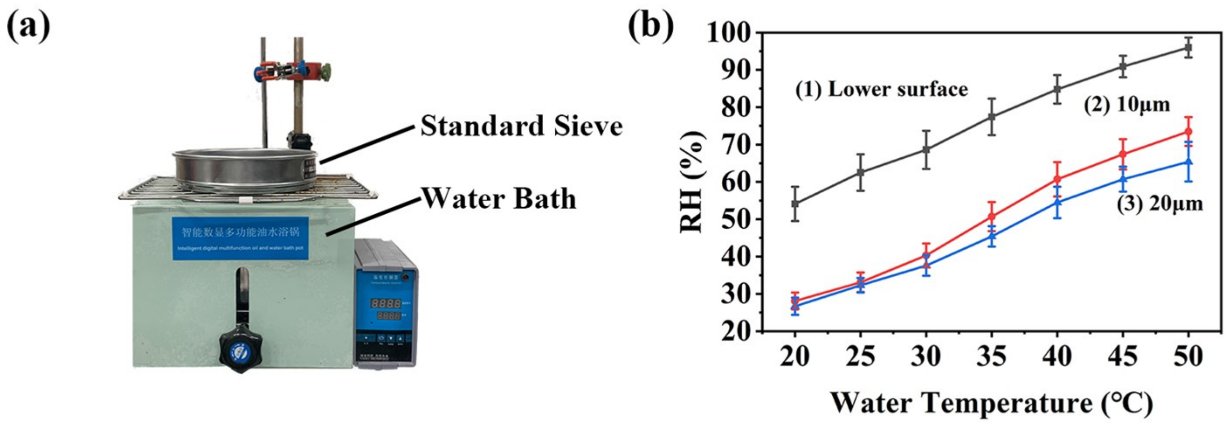

Figure S14. (a) Photograph of experimental setup of water bath for providing humidity gradients at different temperature. (b) Relative humidity of the top and bottom faces of a 10-μm thick 1.5% GO/CMC/Fe^{3+} film at water temperature ranging 20 ℃ to 50 ℃.

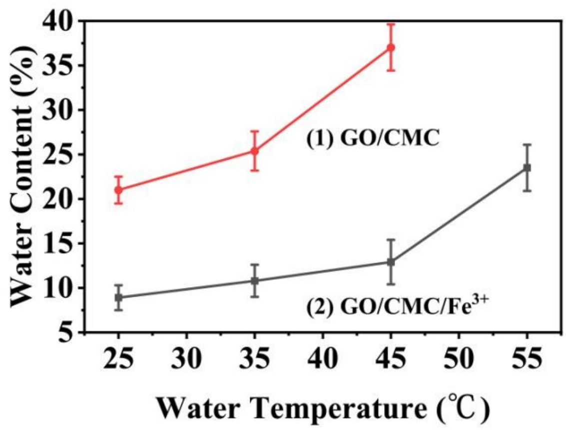

Figure S15. Saturated water content for 15-μm 1.5% GO/CMC film and 15-μm 1.5% GO/CMC/Fe^{3+} film on the porous moist substrate suspended 1.0 cm above water surface at different temperature.

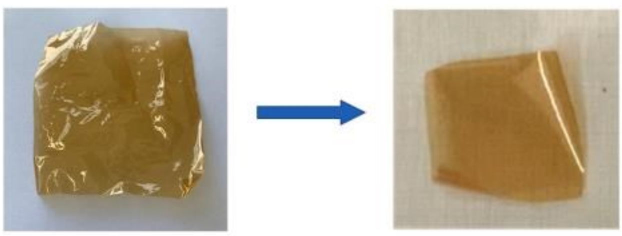

Figure S16. The uneven film could be flattened by repeated training on the moist substrate and then showed fast flipping motion.

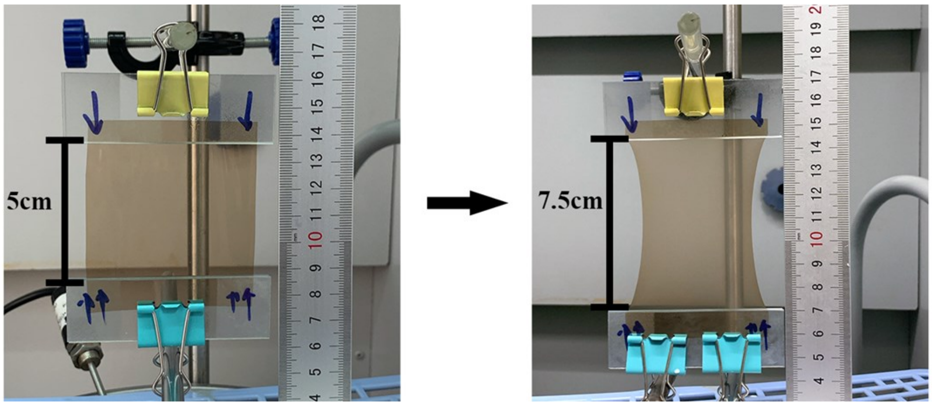

Figure S17. Snapshots of pre-stretching treatment of GO/CMC film suspended above water bath at 75°C.

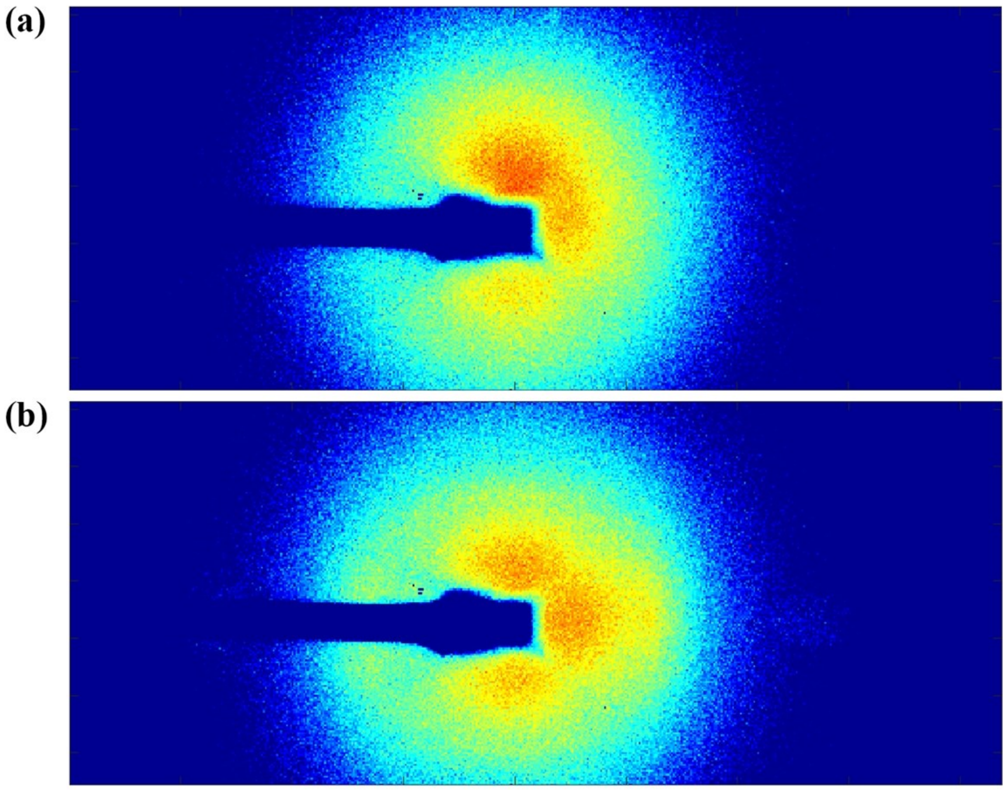

Figure S18. 2D XRD patterns for (a) unstretched film actuator, (b) pre-stretched film actuator.

Despite the pre-stretching process bring influences on the strength and humidity response performance of the film actuator. There is no obvious difference between the 2D XRD patterns of the unstretched film actuator and pre-stretched film actuator[6]. However, both the tensile strength and modulus of the treated film increased about 1.10 and 1.20 times after being stretched (**Figure S19** and **Table S1**). More importantly, the treated film actuators had anisotropic humidity response performance. On a horizontal substrate, the stretched actuator only flipped in the direction perpendicular to its pre-stretching direction (**Figure S20b** and **Video 11**) while the control sample without pre-stretching flipped alternately in the direction of length and width (Figure S20a and Video 11).

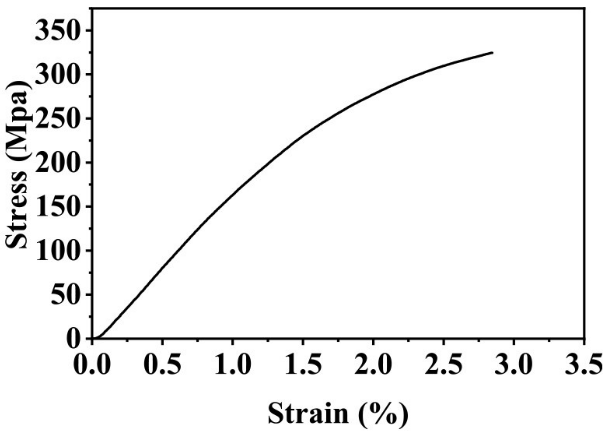

Figure S19. Typical stress-strain curves of GO/CMC/Fe^{3+} film with prestretching.

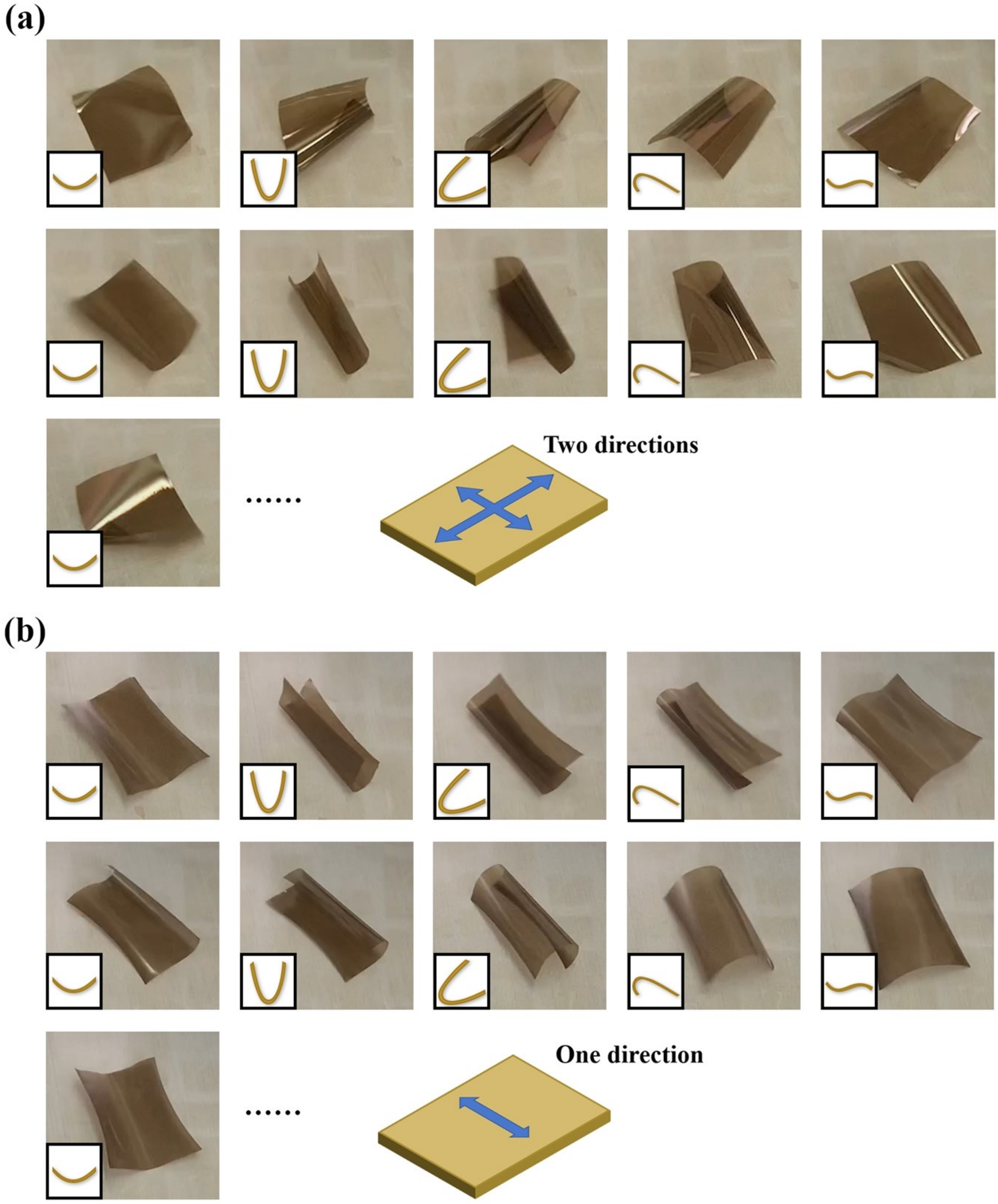

Figure S20. (a) The actuator without pre-stretching flips alternately in the direction of length and width; (b) The actuator with pre-stretching only flips in the direction perpendicular to its pre-stretching direction.

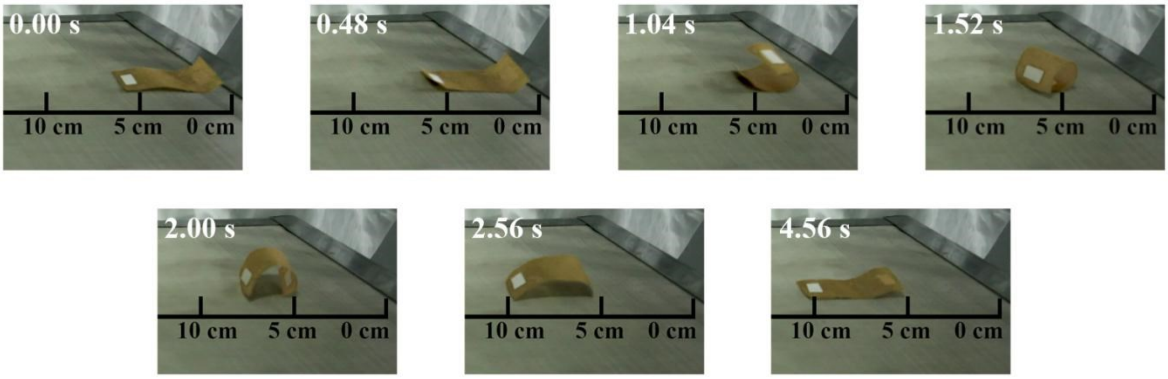

Figure S21. Sequential snapshots showing a locomotive cycle from right to left for the soft robot within 4.56 s.

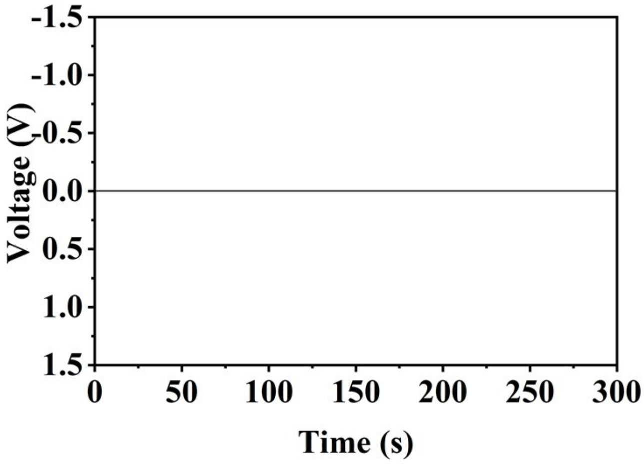

Figure S22. Output voltage of a generator without the actuator.

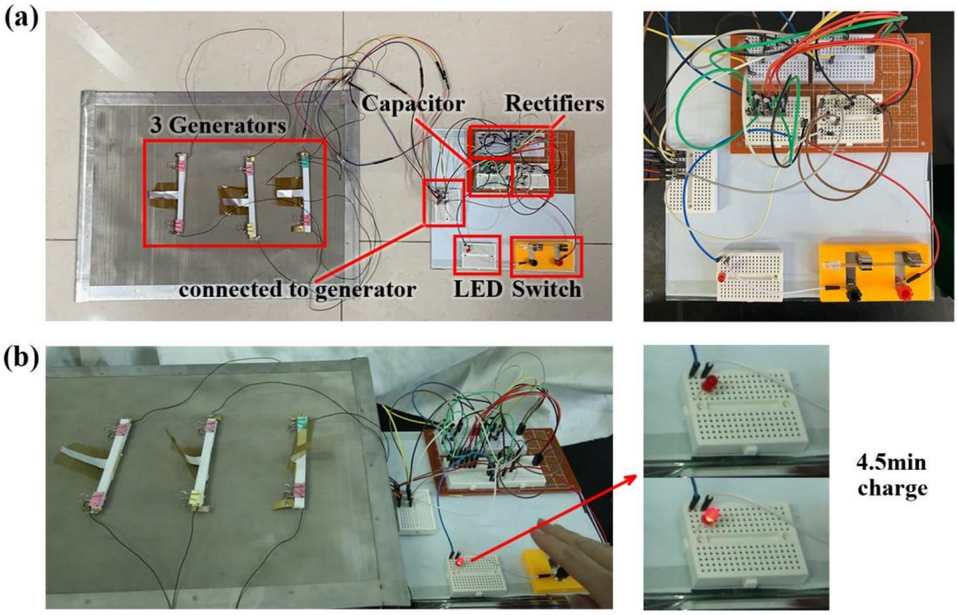

Figure S23. (a) Photographs of electricity generation setup connected with generator, rectifier, capacitor and LET. (b) After a 4.5-minute charge, a LED can be lit by three capacitors in series.

Table S1. The tensile strength and modulus of the moist 1.5% GO/CMC, CMC, moist 1.5% GO/CMC/Fe^{3+}, CMC/Fe^{3+}, 1.5% GO/CMC, 1.5% GO/CMC/Fe^{3+} films, and 1.5% GO/CMC/Fe^{3+} film with prestretching

Films	Fracture strain	Modulus
Moist GO/CMC	63.1±7.3 Mpa	0.70±0.13Gpa
CMC	96.6±5.0 Mpa	2.44±0.10Gpa
Moist GO/CMC/Fe^{3+}	182.3±15.6Mpa	4.68±0.34Gpa
CMC/Fe^{3+}	190.8±13.3Mpa	6.15±0.25Gpa
GO/CMC	208.8±16.7Mpa	7.23±0.28Gpa
GO/CMC/Fe^{3+}	294.4±18.2Mpa	9.53±0.36Gpa
GO/CMC/Fe^{3+} after stretched	324.5±19.8 MPa	11.52±0.42 GPa

2. Supporting Video Captions

Video S1. The flipping motion of the two films with different thickness (10 μm and 20 μm) at water temperature ranging 15℃ to 85 ℃.

Video S2. The continuous flipping motion for 25 min of the 10-μm thick film at 40 ℃ and the 20-μm thick film at 50 ℃.

Video S3. Comparison of the flipping ability for the 10-μm thick film at 40 ℃ before and after Fe(III) crosslinking.

Video S4. The uneven film failed to perform the flipping motion before flattening, but the flattened film could conduct the rapid flipping motion.

Video S5. The flipping motion of the 10-μm thick film on palm.

Video S6. The continuous oscillatory motion of the 20-μm thick film for 20 min.

Video S7. The stretched alignment film actuator underwent the downward directional turnover on the moist substrate by natural evaporation with an inclination angle of 15° with the help of gravity, while the control sample without prestretching failed to flip straightly along the slope.

Video S8. The stretched film attached two white tapes could served as a soft robot undergoing rolling motion from right to left and the robot could cover the 40-cm distance.

Video S9. The single experimental setup with a PVDF element for electricity generation based on hydro-induced actuation of the film.

Video S10. The experimental setup and the process to power a red LED within 4.5 min of charging through natural water evaporation.

Video S11. The stretched actuator only flips in the direction perpendicular to its pre-stretching direction while the control sample without pre-stretching flips alternately in the direction of length and width.

3.References

1 K. Shahzadi, I. Mohsin, L. Wu, X. Ge, Y. Jiang, H. Li and X. Mu, *ACS Nano*, 2017, **11**, 325–334.

2 R. K. Layek, A. Kundu and A. K. Nandi, *Macromolecular Materials and Engineering*, 2013, **298**, 1166–1175.

3 X. Zhao, Q. Zhang, D. Chen and P. Lu, *Macromolecules*, 2010, **43**, 2357–2363.

4 X. Yang, Y. Tu, L. Li, S. Shang and X. Tao, *ACS Appl. Mater. Interfaces*, 2010, **2**, 1707–1713.

5 J. Liang, Y. Huang, L. Zhang, Y. Wang, Y. Ma, T. Guo and Y. Chen, *Advanced Functional Materials*, 2009, **19**, 2297–2302.

6 B. Li, P. I. Xidas and E. Manias, *ACS Appl. Nano Mater.*, 2018, **1**, 3520–3530.